Stability, critical fluctuations and $1/f^{\alpha}$-activity of neural fields involving transmission delays

A. Hutt*
Weierstrass-Institute for Applied Analysis and Stochastics
Mohrenstr.39, 10117 Berlin, Germany†

T.D. Frank‡
Institute for Theoretical Physics, University of Münster,
Wilhelm-Klemm-Str. 9, 48149 Münster, Germany
(Dated: July 15, 2004)

This work studies the stability and the stochastic properties of neural activity evoked by external stimulation. The underlying model describes the spatiotemporal dynamics of neural populations involving both synaptic delay and axonal transmission delay. We show, that the linear model recasts to a set of affine delay differential equations in spatial Fourier space. Besides a stability study for general kernels and general external stimulation, the power spectrum of evoked activity is derived analytically in case of external Gaussian noise. Further applications to specific kernels reveal critical fluctuations at Hopf- and Turing bifurcations and allow the numerical detection of $1/f^{\alpha}$-fluctuations near the stability threshold.

PACS numbers: 87.19.La ; 02.30.Ks ; 02.30.Oz ; 02.50.Sk ; 05.40.Ca

I. INTRODUCTION

Random fluctuations have been reported in spatially-extended systems in biology, chemistry and physics [1–3]. These fluctuations origin from thermal activity or unpredictable chaotic activity [4] and may yield novel effects as stochastic or coherence resonance [5] or noise-induced transitions [6]. In neural systems, background fluctuations are supposed to originate from spontaneous synaptic activity [7], while their spectral properties define the responsiveness of the neurons in the system [8]. In this context, several studies showed the importance of $1/f^{\alpha}$-noise on both microscopic [9, 10] and macroscopic level [11, 12]. There are various effects of fluctuations on neural properties and we mention stochastic resonance enhancement measured in neocortical pyramidal cells [13] and modeled by induced $1/f$ noise [14] and more general distributed noise sources [15]. In addition, noise may facilitate the detection of subthreshold neural activity [16, 17]. The origins of long memory activity as $1/f^{\alpha}$-noise is not fully understood yet. However, several mechanisms have been found [18], for example the superposition of relaxation processes [19], noise in diffusion processes [20], clustering of signal pulses [21] and nonlinear processes with fractal characteristics [22]. Further Usher and Stemmler [9] explained $1/f$-fluctuations in neural systems by pattern formation in neural populations subject to uncorrelated noise.

In addition to the spectral properties of fluctuations, some studies examined the change of their statistical properties while changing experimental conditions. For instance, Wallenstein et al. [23] examined electroencephalographic data obtained during a triggered motor coordination experiment, which reveals a phase transition in finger movements [24]. Examinations of the occuring fluctuations revealed large fluctuation variances near the phase transition threshold both in the brain signals and the behavioral data. These critical fluctuations are well-known from the theory of phase transitions. Several studies have modeled successfully this macroscopic phase transition and the corresponding critical fluctuations by mesoscopic population models [25–27]. Apart from these findings, further previous studies also indicate large-scale coherent phenomena in neural pathologies, which originate from mutual neural population activity. Examples are the hand tremor in Parkinson disease [28], epileptic seizures [29] or hallucinations [30]. The latter in some cases exhibits a shift of the neural state to an instability by increased neuronal excitation [31]. Some studies explained visual hallucination patterns by stability loss in neural populations at bifurcation points [32, 33]. However, the mentioned neural models only treat a single time scale, namely the synaptic delay time. In contrast more recent approaches examine the stability of neural population fields involving constant delayed feedback [34–36] or axonal transmission delay [37–42]. To our best knowledge, most of the latter stability studies neglect random fluctuations. However, these mesoscopic fluctuations may yield $1/f^{\alpha}$-activity or explain macroscopic critical fluctuations as mentioned above and thus are necessary for realistic descriptions of neural systems.

The present work complements previous studies by considering a population model involving transmission delay subjected to external fluctuations. The subsequent section introduces the neural field model and discusses

*Electronic address: hutt@wias-berlin.de
†Supported by the DFG research center "Mathematics for key technologies" (FZT 86) in Berlin, Germany.
‡Electronic address: tdfrank@uni-muenster.de

briefly its properties. Section III discusses the stability and the power spectrum of the field for general connectivity kernels. In the subsequent section, we examine specific synaptic kernels and find critical fluctuations in case of Hopf and Turing instabilities. Further, long memory activity is detected for excitatory diffusive fields. The last section discusses the obtained results and closes the work.

II. THE FIELD MODEL

The present work treats activity in a spatially-extended field of neural populations, which gives the neural activity coarse-grained in space and time [43, 44]. This approach is reasonable for slow synapses at temporal scales $\sim 5-10$ms, high firing rates $>\sim 200$Hz and a mesoscopic spatial scale of a few millimeters [45]. Our model assumes a single neuron type and excitatory and inhibitory chemical synapses with corresponding efficacies g_e and g_i, respectively, while the transmission delay along dendritic structures is negligible. The synapses sum up all lateral contributions weighted by the synaptic connectivity kernels f_e and f_i for excitatory and inhibitory connections, respectively. These kernels represent probability density distributions of synaptic connection and thus are normalized to unity. Furthermore finite axonal speeds $v_{e,i}$ yield the transmission delay $\Delta_{e,i} = |x-y|/v_{e,i}$ between two locations x and y. Since chemical synapses respond to incoming activity by temporal delay, the excitatory and inhibitor post-synaptic potentials $V_{e,i}$ at spatial position x and time t obey

$$V_{e,i}(x,t) = \int_{-\infty}^{t} d\tau h(t-\tau) \times \left[g_{e,i} \int_\Gamma dy\ f_{e,i}(x-y) S[V(y,\tau-\Delta_{e,i})] + I_{e,i}(x,\tau) \right], \tag{1}$$

with the synaptic impulse response function $h(t)$, $V = V_e - V_i$ and the external excitatory and inhibitory inputs I_e and I_i, respectively. The transfer function $S[V]$ originates from the statistical distribution of firing thresholds and owns a sigmoidal shape in case of unimodal distributions. Eventually post-synaptic potentials sum up at the soma and the final model equation for the somatic membrane potential V reads

$$\begin{aligned} V(x,t) &= \hat{I}_t \int_\Gamma dy\ K_e(x-y) S[V(y,t-\Delta_e)] \\ &\quad - K_i(x-y) S[V(y,t-\Delta_i)] + \hat{I}_t\ I(x,t), \end{aligned} \tag{2}$$

with $K_e = g_e f_e$, $K_i = g_i f_i$, $I = I_e - I_i$ and the convolution operator $\hat{I}_t$ acting on the test function $f(t)$ like $\hat{I}_t f(t) = \int_{-\infty}^{t} d\tau h(t-\tau) f(\tau)$.

Most cortical areas are part of neural modular network and receive external connections from other brain areas. Well-known examples are the cortico-thalamical subnetwork [46] studied in the context of sleep cycles and the projection from the lateral geniculate nucleus to the visual cortex important in visual perception. First we assume external excitatory stimulation I_0 constant in space and time. Then, the stationary constant field $V(x,t) = V_0$ obeys $V_0 = (g_e - g_i) S[V_0] + I_0$. Considering the external stimulus I_0 as control parameter, the corresponding bifurcation diagram exhibits either hysteresis with two stable and one unstable state or owns a single stable state V_0 (cf. [39]). We mention the similarity to the cusp catastrophy [47].

Now, we considering small deviations $u(x,t) = V(x,t) - V_0 \ll V_0$ about the stationary solution V_0 and assume the additional external stimulus $s(x,t) \ll I_0$. Thus Eq. (2) reads

$$\begin{aligned} u(x,t) &= \hat{I}_t\ \gamma \int_\Gamma dy\ K_e(x-y) u(y,t-\Delta_e) \\ &\quad - K_i(x-y) u(y,t-\Delta_i) + \hat{I}_t\ s(x,t). \end{aligned} \tag{3}$$

Here, $\gamma = \delta S/\delta V$ at $V = V_0$ depends implicitly on I_0, while $\delta/\delta V$ denotes the functional derivative. Hence γ represents the control parameter for the linear case. The external stimulus $s(x,t)$ may correspond to a deterministic driving force, e.g. originating from sensoric perception. Alternatively, $s(x,t)$ may describe a fluctuating force acting on the neural field caused by synaptic fluctuations. In fact, in Sec. IV we will use Eq. (3) to study the stochastic evolution of $u(x,t)$ under the impact of a fluctuating force.

Since

$$\begin{aligned} &K_{e,i}(x-y) u(y,t-\Delta_{e,i}) = \\ &\int_{-\infty}^{t} d\tau\ K_{e,i}(x-y) \delta(t-\tau-\Delta_{e,i}) u(y,\tau) \\ = &\int_{-\infty}^{t} d\tau\ n_{e,i}(x-y,t-\tau) u(y,\tau), \end{aligned}$$

where $\delta(\cdot)$ denotes the delta distribution, the Fourier transform of Eq. (3) reads

$$\begin{aligned} \tilde{u}(k,t) &= \frac{1}{\sqrt{2\pi}} \int_{-\infty}^{+\infty} dx\ u(x,t) e^{-ikx} \\ &= \hat{I}_t \left[\gamma\sqrt{2\pi} \int_0^\infty d\tau \tilde{n}(k,\tau) \tilde{u}(k,t-\tau) + \tilde{s}(k,t) \right]. \end{aligned} \tag{4}$$

Here, $\tilde{u}, \tilde{s}$ and $\tilde{n}$ represent the Fourier transforms of u, s and $n = n_e - n_i$, respectively. Hence, in the linear regime the spatio-temporal dynamics of the neural field decouples into single modes in k-space, while the space-dependant propagation delay transforms to a distribution of constant delays.

Finally assuming a symmetric kernel Eq. (4) reads

$$\begin{aligned}\tilde{u}(k,t) &= \hat{I}_t\ 2\gamma \int_0^\infty d\tau\ (v_e K_e(v_e\tau)\cos(kv_e\tau) \\ &\quad -v_i K_i(v_i\tau)\cos(kv_i\tau))\tilde{u}(k,t-\tau) \\ &\quad +\hat{I}_t\ \tilde{s}(k,t) \end{aligned} \tag{5}$$

III. STABILITY ANALYSIS AND POWER SPECTRUM FOR GENERAL KERNELS

In this section, we set $K_i = 0$, $K_e = K$ and $v_e = v$ without loss of generality. Let us assume the inverse operator $\hat{I}_t^{-1} = \hat{L}(\partial/\partial t)$ exists, such that

$$\hat{L}(\partial/\partial t)\ h(t) = \delta(t),$$

while $h(t)$ is taken from (1). Then Eq. (5) becomes an affine delay differential equation with distributed delays

$$\begin{aligned}\hat{L}(\partial/\partial t)\tilde{u}(k,t) &= 2v\gamma \int_0^\infty d\tau\ K(v\tau)\cos(kv\tau)\tilde{u}(k,t-\tau) \\ &\quad +\tilde{s}(k,t)\ . \end{aligned} \tag{6}$$

Its general solution is

$$\tilde{u}(k,t) = \tilde{u}_h(k,t) + \int_{-\infty}^{+\infty} dt'\ G(k,t-t')s(k,t')\ , \tag{7}$$

where $\tilde{u}_h(k,t)$ represents the homogeneous solution of (6) and $G(k,t-t')$ represents the Greens function. Applying standard techniques in linear response theory, the Greens function is given by

$$G(k,t) = \frac{1}{2\pi}\int_{-\infty}^{+\infty} d\omega \frac{e^{-i\omega t}}{L(i\omega) - \bar{K}(k,i\omega)}, \tag{8}$$

where $\hat{L}\exp(-i\omega t) = L(i\omega)\exp(-i\omega t)$ and

$$\bar{K}(k,i\omega) = 2v\gamma \int_0^\infty d\tau\ K(v\tau)\cos(kv\tau)e^{i\omega\tau}.$$

Extending the real domain of ω to the complex plane and applying the residue theorem, it is

$$G(k,t) = \Theta(t)\left[i\sum_{l=1}^{m} Res_l(e^{-i\Omega_l t})\right] = \Theta(t)\sum_{l=1}^{m} r_l e^{\lambda_l(k)t} \tag{9}$$

.

with the Heaviside function $\Theta(\cdot)$. Here, m denotes the number of complex roots $\Omega_l(k) \in \mathcal{C}$ of the denominator in (8), it is $\lambda_l(k) = i\Omega_l(k)$ and Res_l denotes the residue of the numerator in Eq. (8) at root $\Omega_l(k)$. The constants $r_l \in \mathcal{C}$ are fixed by the corresponding residues. We remark that the vanishing denominator in (8) corresponds to the characteristic equation known from theory of delayed differential equations. Further, infinite transmission speed leads to

$$L(i\Omega) = 2\gamma \int_0^\infty K(s)\cos(ks)ds$$

and m is given by the order of $\hat{L}$.

Eventually, inserting Eq. (9) into Eq. (7), the solution of (6) reads

$$\tilde{u}(k,t) = \tilde{u}_h(k,t) + \sum_{l=1}^{m} r_l \int_0^t dt'\ e^{\lambda_l(k)(t-t')}\tilde{s}(k,t'), \tag{10}$$

assuming the stimulus onset at $t = 0$. If all roots are located in the lower complex plane, i.e. $Im(\Omega_l(k)) = Re(\lambda_l(k)) < 0$, Eq. (10) owns stable solutions for bounded deterministic stimuli and random fluctuations described by a Lévy process in case of finite kernels [48].

As mentioned in the introduction, $1/f^\alpha$-fluctuations have been found in neural populations. To detect this behavior in our model, the subsequent part discusses briefly the temporal power spectrum of the resulting field $u(x,t)$. The Fourier back transformation of (10) yields

$$\begin{aligned}u(x,t) &= \tilde{u}_h(x,t) \\ &\quad + \frac{1}{\sqrt{2\pi}}\sum_{l=1}^{m} r_l \int_0^t dt' \int_{-\infty}^{\infty} e^{\lambda_l(k)(t-t')}\tilde{s}(k,t')e^{ikx}dk, \end{aligned}$$

while $\tilde{u}_h(x,t)$ represents the homogeneous solution of Eq. (3). Now considering external uncorrelated Gaussian noise with $\langle\tilde{s}(k,t)\rangle = 0$ and $\langle\tilde{s}(k,t)\tilde{s}(k',t')\rangle = Q\delta(k-k')\delta(t-t')$, the autocorrelation function reads

$$\begin{aligned}C(t,\tau) &= \langle u^*(x,t)u(x,\tau)\rangle \\ &= \frac{Q}{2\pi}\sum_{l=1}^{m} r_l \int_{-\infty}^{\infty} P_l(k)e^{\lambda_l(k)|\tau-t|}dk \end{aligned} \tag{11}$$

with

$$P_l(k) = -\sum_{j=1}^{m}\frac{r_j^*}{\lambda_j^*(k)+\lambda_l(k)}.$$

Here, Q measures the overall strength of the fluctuation force, $\langle\cdot\rangle$ represents the ensemble average and $*$ denotes the complex conjugate. In addition, Eq. (11) assumes $t, \tau \to \infty$. Now, according to the Wiener-Khinchine theorem [49] the power spectrum reads

$$S^2(\omega) = \frac{-2Q}{\sqrt{2\pi}^3}\sum_{l=1}^{m} r_l \int_{-\infty}^{\infty} \frac{\lambda_l(k)}{\omega^2+\lambda_l^2(k)}P_l(k)dk. \tag{12}$$

The function $P_l(k)$ gives the distribution of time scales $1/\lambda_l(k)$. Recalling the origins of $1/f^\alpha$-activity [18], these multiple time scales may yield regimes of $S^2(\omega) \sim 1/\omega^\alpha$. Subsequently, the presence of $1/f^\alpha$-activity in the present system depends mainly on the synaptic connectivity kernels $K_{e,i}$ and the synaptic and axonal intrinsic time scales defined by $h(t)$ and $v_{e,i}$, respectively. Closer investigations follow in subsection IV C for specific kernels.

IV. SPECIFIC SYNAPTIC CONNECTIVITY AND STOCHASTIC FORCE

The present section discusses the case of the exponential impulse response $h(t) = \exp(-t/\tau)$, i.e. $\hat{L}_t = \partial/\partial t + \tau$. The parameter τ represents the synaptic time scale. Furthermore, we assume that the neural field is driven by a fluctuating force. That is, we put

$$s(x,t) = \sqrt{Q}\Gamma(x,t) \ , \tag{13}$$

where $\Gamma(x,t)$ corresponds to a Gaussian distributed fluctuating force that is uncorrelated in space and time like $\langle\Gamma(k,t)\rangle = 0$, $\langle\Gamma(k,t)\Gamma(k',t')\rangle = 2\delta(t-t')\delta(k-k')$ [49]. The parameter Q represents the noise amplitude.

A. Hopf bifurcation

In a first case, we specify the synaptic connectivity to local excitation at a short range and lateral inhibition at a fixed distance, i.e. the kernels in (3) read

$$K_e(x) = \frac{g_e}{2\sqrt{D}} e^{-|x|/\sqrt{D}} \quad , \quad K_i(x) = \frac{g_i}{2}\delta(x-|R|).$$

Here, $\sqrt{D}$ and R represent the excitatory and inhibitory spatial scale, respectively. For $\sqrt{D} \ll 1$ and $\sqrt{D}/v_e \ll \tau$, the excitatory propagation delay is negligible yielding [50]

$$\begin{aligned}
&\int_{-\infty}^{+\infty} dy\ K_e(x-y)u(y,t-\Delta_e) \\
&\approx \left(1 + \frac{1}{2}\int_{-\infty}^{\infty} dz\ K(z)z^2\ \frac{\partial^2}{\partial x^2}\right) u(x,t) \\
&= \left(1 + D\frac{\partial^2}{\partial x^2}\right) u(x,t).
\end{aligned}$$

Hence, the local excitatory coupling is equivalent to diffusive coupling with diffusion coefficient D.

Following the analysis steps in section II the corresponding delay differential equation in Fourier space becomes

$$\begin{aligned}
\frac{\partial}{\partial t}\tilde{u}(k,t) \ &= \ \left[\gamma g_e(1-Dk^2) - \tau\right]\tilde{u}(k,t) \\
&- \ \gamma g_i \cos(kR)\tilde{u}(k,t-t_0) + \sqrt{Q}\,\Gamma(k,t)
\end{aligned} \tag{14}$$

with the delay $t_0 = R/v_i$. Thus the system includes two time scales, namely the synaptic delay time τ and the propagation delay time t_0. Introducing the parameters

$$a(k) = \tau - \gamma g_e + \gamma g_e D k^2 \ , \ b(k) = \gamma g_i \cos(kR) \ , \tag{15}$$

Eq. (14) can be written as

$$\frac{\partial}{\partial t}\tilde{u}(k,t) = -a(k)\tilde{u}(k,t) - b(k)\tilde{u}(k,t-t_0) + \sqrt{Q}\,\Gamma(k,t). \tag{16}$$

That is, we deal with a linear stochastic delay differential equation for the Fourier amplitudes $\tilde{u}(k,t)$ that involves k-dependent parameters. Let us discuss Eq. (14) in the context of the emergence of oscillatory behavior. To this end, we first examine the behavior of the spatially homogeneous Fourier mode with $k = 0$. We have $a(0) = \tau - \gamma g_e$ and $b(0) = \gamma g_i$. For $k = 0$ and $a(0) \geq b(0) > 0$ Eq. (16) describes a stable system both in the deterministic ($Q = 0$) [51, 52] and the stochastic case ($Q > 0$) [53–56]. Therefore, we assume that $b(0) > a(0) > 0$. Then, for $k = 0$ and $Q = 0$ the linear model (16) exhibits a stable (unstable) fixed point $\tilde{u}_{\rm st}(0) = 0$ for delays t_0 smaller (larger) than the critical delay

$$t_{0,\rm c} = \frac{1}{\sqrt{b(0)^2 - a(0)^2}} \arccos\left(-\frac{a(0)}{b(0)}\right) \ . \tag{17}$$

At $t_0 = t_{0,c}$ there is a Hopf bifurcation [51, 52]. Likewise, for $k = 0$ and $Q > 0$ Eq. (16) exhibits stationary distributions for delays $t_0 < t_{0,c}$, whereas for delays $t_0 > t_{0,c}$ stationary distributions do not exist [53–56]. The stationary distributions for $t_0 < t_{0,c}$ correspond to Gaussian distributions with vanishing mean and variance σ^2 defined by

$$\sigma^2 = \frac{Q}{2}\frac{[1+\sqrt{b^2(0)-a^2(0)}]^{-1} b(0)\sin[\sqrt{b^2(0)-a^2(0)}t_0]}{a(0)+b(0)\cos[\sqrt{b^2(0)-a^2(0)}t_0]} \ , \tag{18}$$

It is clear from Eq. (18) that σ^2 becomes infinite at the bifurcation point. Furthermore, from Eq. (16) it follows that the first moment $M_1 = \langle\tilde{u}(0,t)\rangle$ evolves like

$$\frac{\rm d}{{\rm d}t}M_1(t) = -a(0)M_1(t) - b(0)M_1(t-t_0) \ . \tag{19}$$

Eq. (19) can be treated just as Eq. (16) for $Q = 0$. That is, Eq. (19) describes a Hopf bifurcation and for $t_0 > t_{0,c}$ the first moment M_1 oscillates with a gradually increasing amplitude. Next, let us consider Fourier modes with nonvanishing k-values. To this end, we need to distinguish between two cases: $|k|R \leq \pi/2$ and $|k|R > \pi/2$. In the first case, we have $a(k) > a(0)$ and $b(k) < b(0)$. Consequently, if the homogeneous Fourier mode is stable, then all Fourier modes with $|k|R \leq \pi/2$ are stable. In the second case, we assume that the diffusion coefficient D satisfies the inequality $g_e D k^2 \geq g_i$ for $|k|R > \pi/2$, which implies that $a(k) > b(k)$ holds (e.g. one may choose $D = 4g_iR^2/[g_e\pi^2]$). Then, the Fourier modes with $|k|R > \pi/2$ are stable as well.

Taking a neurophysiological point of view, it is of particular interest to study the impact of the control parameter γ (see Sec. II). From Eq. (17) it follows that the critical parameter γ_c is given by

$$t_0\sqrt{\gamma_c^2 g_i^2 - (\tau - \gamma_c g_e)^2} = \cos\left(-\frac{\tau - \gamma_c g_e}{\gamma_c g_i}\right) \ . \tag{20}$$

In sum, for delays $t_0 < t_{0,c}$ or control parameters $\gamma < \gamma_c$ all Fourier modes described by Eq. (16) correspond to stable modes that have in the deterministic case stable fixed points at $\tilde{u}_{\rm st}(k) = 0$ and exhibit

in the stochastic case Gaussian stationary distributions with vanishing mean and variance

$$\sigma^2(k) = \frac{Q}{2}\frac{1 + w^{-1}(k)b(k)\sin[w(k)t_0]}{a(k) + b(k)\cos[w(k)t_0]} \tag{21}$$

where $w(k)$ is defined by

$$w(k) = \sqrt{b^2(k) - a^2(k)} \tag{22}$$

(note that Eq. (21) holds even if w corresponds to an imaginary value [57]). As a result, the neural field is spatially homogeneous. For $t_0 \to t_{0,c}$ or $\gamma \to \gamma_c$ the variance of the amplitude of the homogeneous Fourier mode with $k = 0$ becomes infinite, whereas the variances of all other Fourier amplitudes are still finite, see also Fig. 1. In this sense the neural field exhibits critical fluctuations at the bifurcation point. If $t_0 = t_{0,c} + \epsilon$ or $\gamma = \gamma_c + \epsilon$ with ϵ positive and small, then the amplitude $\tilde{u}(0,t)$ and amplitudes $\tilde{u}(k,t)$ with small k-values become unstable and the first moments $M_1(k,t) = \langle\tilde{u}(k,t)\rangle$ of these modes oscillate with gradually increasing amplitudes, see Fig. 2. Consequently, constant oscillations emerge in the neural field and we deal with critical fluctuations at the bifurcation point of constant waves.

Insert Figures 1 and 2 about here.

B. Turing bifurcation

Now, we discuss the case of local excitation and lateral inhibition in intracortical fields (cf. [38]). That is, we use

$$K_e(x) = \frac{g_e}{2r_e}e^{-|x|/r_e} \quad , \quad K_i(x) = \frac{g_i}{2r_i}e^{-|x|/r_i},$$

where $r_{e,i}$ denote the excitatory and inhibitory spatial ranges with $r_e < r_i$. Using $\hat{L}_t = \partial/\partial t + \tau$ and $v_e = v_i = v$, Eq. (6) becomes

$$\begin{aligned}&\frac{\partial}{\partial t}\tilde{u}(k,t) = -\tau\tilde{u}(k,t)\\ &+v\gamma\int_0^\infty d\tau\left[\frac{g_e}{r_e}e^{-v\tau/r_e} - \frac{g_i}{r_i}e^{-v\tau/r_i}\right]\cos(kv\tau)\tilde{u}(k,t-\tau)\\ &+\sqrt{Q}\,\Gamma(k,t)\ .\end{aligned} \tag{23}$$

The ansatz $\tilde{u}(k,t) = u_k\exp(\lambda t)$ yields the characteristic equation

$$\lambda + \tau = \gamma\left[g_e\frac{1 + \lambda r_e/v}{(1 + \lambda r_e/v)^2 + r_e^2k^2} - g_i\frac{1 + \lambda r_i/v}{(1 + \lambda r_i/v)^2 + r_i^2k^2}\right], \tag{24}$$

which corresponds to a polynomial of 5th order. The first moments $M_1(k,t) = \langle\tilde{u}(k,t)\rangle$ evolve like

$$\begin{aligned}&\frac{\partial}{\partial t}M_1(k,t) = -\tau M_1(k,t)\\ &+v\gamma\int_0^\infty d\tau\left[\frac{g_e}{r_e}e^{-v\tau/r_e} - \frac{g_i}{r_i}e^{-v\tau/r_i}\right]\cos(kv\tau)M_1(k,t-\tau)\,.\end{aligned} \tag{25}$$

In the following, we will discuss the model (23) in the context of a Turing bifurcation [38]. In order to illustrate our main objective, it is sufficient to study a particular parameter set for which the Lyapunov spectrum $\lambda(k)$ exhibits at the critical control parameter γ_c a pair of vanishing Lyapunov exponents $\lambda(k)$ with $k = \pm k_c$ and $k_c > 0$. Figures 3 and 4 show such a spectrum. In line with our general consideration in section III, we can assume that for $\gamma < \gamma_c$ the system is stable. Due to the linearity of the problem, it is reasonable to assume that the amplitudes $\tilde{u}(k,t)$ are distributed like Gaussian distributions with vanishing mean values and finite variances. For $\gamma \to \gamma_c$ the variances of the critical Fourier amplitudes $\tilde{u}(\pm k_c,t)$ become infinite, see also Fig. 5. Finally, for γ slightly larger than γ_c the Fourier amplitudes $\tilde{u}(\pm k,t)$ with $k \approx \pm k_c$ become unstable. Since we deal with a Turing bifurcation point at which the imaginary parts of $\lambda(\pm k_c)$ vanish, from Eq. (25) it follows that the first moments $M_1(k,t)$ with $k \approx \pm k_c$ increase monotonically with time, see Fig. 6. In sum, we deal here with the emergence of a Turing pattern in the neural field and with critical fluctuations at the Turing bifurcation point.

Insert Figures 3, 4, 5, 6 about here.

C. $1/f^\alpha$-fluctuations

Finally, this section discusses the power spectrum of the resulting spatiotemporal field according to the results in section III. The assumed connectivity is local and excitatory with $K(x) = K_e(x)$ taken from section IV A and it is $v = v_e$. In addition, suitable spatial boundary conditions limit the spatial frequency spectrum to $-k_0 \le k \le k_0$. As has been observed in section IV A, this coupling model is equivalent to a diffusion model with diffusion coefficient D.

For large transmission speeds $v \gg |\omega\sqrt{D}|$, the quantities in Eq. (12) read $m = 1$, $r = 1$, $\Omega(k) = -i(1 - g\gamma/(Dk^2+1))$, $P(k) = -(Dk^2+1)/2(Dk^2+1-g\gamma)$. Here, the maximum time scale occurs at $k = 0$ with $\lambda(0) = -(1-\gamma g)$. That is $\gamma_c = 1/g$ represents the critical control parameter. The power spectrum reads

$$S^2(\omega) = \frac{Q}{\pi\sqrt{2\pi D}}\int_{-\bar{k}}^{\bar{k}}\frac{(u^2+1)^2}{\omega^2(u^2+1)^2 + (u^2+1-g\gamma)^2}du \tag{26}$$

with $\bar{k} = k_0/\sqrt{D}$. Figure 7 shows $S^2(\omega)$ for two control parameters. For $\omega < 1$, the plot reveals colored noise $S^2(\omega) \sim 1/\omega^{0.19}$ at the stability threshold $\gamma \approx \gamma_c$, while $\gamma \ll 1/g$ yields white noise with $S^2(\omega) \sim 1/\omega^0$. That is near the stability threshold the autocorrelation exhibits a power law $C(t, t+\tau) \sim \tau^{-0.81}$. For $\omega \to \infty$ the power spectrum shows Brownian fluctuations with $S^2(\omega) \sim 1/\omega^2$ for both control parameters.

In addition, for vanishing spatial coupling $\sqrt{D} \to 0$ the

power spectrum reads

$$S^2(\omega) = \frac{2Qk_0}{\pi D\sqrt{2\pi}} \frac{1}{\omega^2 + (1-g\gamma)^2}. \qquad (27)$$

That is white noise with $S^2(\omega) \approx const$ occurs for $\omega \to 0$ and Brownian motion with $S^2 \sim 1/\omega^2$ is present for large $\omega \gg |1 - g\gamma|$.

Insert Figure 7 about here.

V. DISCUSSION

The previous sections discuss the stability and stochastic properties of evoked neural activity. First we show that the transmission delay in the spatial domain reduces to a distribution of constant delays in the corresponding Fourier domain. Hence, the linear neural field evolves in Fourier-space according to affine delay differential equations. Further investigations on the evoked response to external stimulation reveal that only the characteristic roots of the delay differential equations determine the field stability. In addition, the temporal spectrum of the evoked activity turns out to depend mainly on the distribution of occuring temporal time scales. These findings are valid for general connectivity kernels. In order to learn more about the evoked response to random fluctuations, we discuss the stability and temporal power spectrum in case of specific synaptic connectivities. In a first example, it is shown that short-range excitation is equivalent to diffusive interaction. An additional discrete inhibitory interaction yields a Hopf-bifurcation for the spatially constant mode. We derive the variance of the stationary activity distribution for all Fourier modes and find a divergent fluctuation variance at the bifurcation threshold of the constant mode. Hence, we showed the occurence of critical fluctuations at the oscillatory bifurcation threshold. Similar constant oscillations have been found in deterministic neural networks [58], while the critical fluctuations have been found experimentally in oscillatory neural activity [23]. Further treatments of intracortical fields also reveal critical fluctuations at the threshold of a Turing bifurcation. Eventually, the power spectrum of purely diffusive fields reveals $1/f^\alpha$-fluctuations for small frequencies near the bifurcation threshold, i.e. fractional Gaussian noise. Thus the corresponding autocorrelation obeys a power law. For large frequencies, the spectrum corresponds to a Brownian motion dynamics. Remarkably the noise properties are different far from the bifurcation threshold, where fluctuations show white noise behavior for small frequencies and Brownian motion properties for large frequencies.

Several studies pointed out that $1/f^\alpha$-fluctuations occur in case of multiple time scales. In the present work, these time scales originate from multiple spatial scales. In addition, our work reveals $1/f^\alpha$-fluctuations near the bifurcation threshold only, though the neural system exhibits multiple time scales for a large range of control parameters. This finding points to the importance of criticality in a system [22]. Further the succesful modeling of critical fluctuations in the presence of propagation delay in nonlocal neural models shows accordance to experimental findings and thus supports our mesoscopic model based on neural populations. Future work may include further important neural mechanisms as temporal feedback delay and may focus on neural models of more specific brain areas, e.g. related to motor-coordination experiments.

[1] H. Haken, *Synergetics: Introduction and Advanced topics* (Springer, Berlin, 2004).
[2] A. Nitzan, P. Ortoleva, J. Deutch, and J. Ross, J. Chem. Physics **61**, 1056 (1974).
[3] Y. Kuramoto, *Chemical Oscillations, Waves, and Turbulence* (Dover, Mineola, 2003).
[4] C. Gardiner, *Handbook of Stochastic Methods* (Springer, Berlin, 1983).
[5] B. Lindner, J. Garcia-Ojalvo, A. Neiman, and L. Schimansky-Geier, Phys. Rep. **392**, 321 (2004).
[6] W. Horsthemke and R. Lefever, *Noise-induced transitions : Theory and Applications in Physics, Chemistry, and Biology* (Springer, Berlin, 1984).
[7] D. Paré, E. Shink, H. Gaudreau, A. Destexhe, and E. Lang, J. Neurophysiol. **79**, 1450 (1998).
[8] L. Nowak, M. Sanchez-Vives, and D. McCormick, Cerebral Cortex **7**, 487 (1997).
[9] M. Usher and M. Stemmler, Phys. Rev. Lett. **74**, 326 (1995).
[10] M. Teich, IEEE Trans. Biomed. Eng. **36**, 150 (1989).
[11] D. Gilden, T. Thornton, and M. Mallon, Science **267**, 1837 (1995).
[12] Y. Chen, M. Ding, and J. Kelso, Phys. Rev. Lett. **79**, 4501 (1997).
[13] N. Ho and A. Destexhe, J. Neurophysiol. **84**, 1488 (2000).
[14] D. Nozaki, J. Collins, and Y. Yamamoto, Phys. Rev. E **60**, 4637 (1999).
[15] M. Rudolph and A. Destexhe, Phys. Rev. Lett. **86**, 3662 (2001).
[16] F. Liu, B. Hu, and W. Wang, Phys. Rev. E **63**, 031907 (2001).
[17] P. beim Graben and J. Kurths, Phys. Rev. Lett. **90**, 100602 (2003).
[18] P. Dutta and P. Horn, Rev. Mod. Phys. **53**, 497 (1981).
[19] J. Bernamont, Ann.Phys.(Leipzig) **7**, 71 (1937).
[20] E. Milotti, Phys. Rev. E **51**, 3087 (1995).
[21] B. Kaulakys and T. Meskauskas, Phys. Rev. E **58**, 7013 (1998).
[22] P. Bak, C. Tang, and K. Wiesenfeld, Phys. Rev. Lett. **59**, 381 (1987).
[23] G. V. Wallenstein, J. A. S. Kelso, and S. L. Bressler, Physica D **84**, 626 (1995).

[24] H. Haken, J. A. S. Kelso, and H. Bunz, Biol. Cyb. **51**, 347 (1985).
[25] V. Jirsa and H. Haken, Phys. Rev. Lett. **7**, 960 (1996).
[26] T. Frank, A. Daffertshofer, P. Beek, and H. Haken, Physica D **127**, 233 (1999).
[27] T. Frank, A. Daffertshofer, C. Peper, P. Beek, and H. Haken, Physica D **144**, 62 (2000).
[28] P. Tass, *Phase resetting in medicine and biology : stochastic modelling and data analysis* (Springer, Berlin, 1999).
[29] F. H. L. da Silva, W. Blanes, S. Kalitzin, J. Parra, P. Suffczynski, and D. V. is, Epilepsia **44**, 72 (2003).
[30] J. R. Brasic, Percep. Motor Skills **86**, 851 (1998).
[31] S. H. Isaacson, J. Carr, and A. J. Rowan, Neurol. **43**, 1619 (1993).
[32] G. B. Ermentrout and J. D. Cowan, Biol. Cybern. **34**, 137 (1979).
[33] P. Tass, J. Biol. Phys. **23**, 21 (1997).
[34] D. Golomb and G. Ermentrout, Network: Comput. Neural Syst. **11**, 221 (2000).
[35] D. Pinto and G. Ermentrout, SIAM J. Applied Math. **62**, 206 (2001).
[36] D. Pinto and G. Ermentrout, SIAM J. Applied Math. **62**, 226 (2001).
[37] P. Nunez, *Neocortical dynamics and human EEG rhythms* (Oxfoord University Press, New York - Oxford, 1995).
[38] A. Hutt, M. Bestehorn, and T. Wennekers, Network: Comput. Neural Syst. **14**, 351 (2003).
[39] F. M. Atay and A. Hutt, SIAM J. Appl. Math. **in press** (2004).
[40] S. Crook, G. Ermentrout, M. Vanier, and J. Bower, J. Comput. Neurosci. **4**, 161 (1997).
[41] W. Freeman, Int. J. Bif. Chaos **10**, 2307 (2000).
[42] S. Coombes, G. Lord, and M. Owen, Physica D **178**, 219 (2003).
[43] H. Wilson and J. Cowan, Kybernetik **13**, 55 (1973).
[44] V. Jirsa and H. Haken, Physica D **99**, 503 (1997).
[45] W. Freeman, Int. J. Bif. Chaos **2**, 451 (1992).
[46] M. Steriade, D. McCormick, and T. Sejnowski, Science **262**, 679 (1993).
[47] J. Cowan and G. Ermentrout, in *Studies in mathematical biology, part I: Cellular behavior and the development of pattern*, edited by S. Levin (MAA, Washington DC, 1978), pp. 67–117.
[48] A. Gushchin and U. Kuechler, Stochastic Proc. Appl. **88**, 195 (2000).
[49] H. Risken, *The Fokker-Planck equation — Methods of solution and applications* (Springer, Berlin, 1989).
[50] J. Murray, *Mathematical Biology* (Springer-Verlag, Berlin, 1989).
[51] R. D. Driver, *Ordinary and delay differential equations — Applied mathematical sciences Vol. 20* (Springer, New York, 1977).
[52] J. K. Hale and S. M. V. Lunel, *Introduction to functional differential equations* (Springer, Berlin, 1993).
[53] U. Küchler and B. Mensch, Stoch. Stoch. Rep. **40**, 23 (1992).
[54] M. C. Mackey and I. G. Nechaeva, Phys. Rev. E **52**, 3366 (1995).
[55] T. D. Frank and P. J. Beek, Phys. Rev. E **64**, 021917 (2001).
[56] T. D. Frank, P. J. Beek, and R. Friedrich, Phys. Rev. E **68**, 021912 (2003).
[57] T. D. Frank, Phys. Rev. E **69**, 061104 (2004).
[58] M. Earl and S. Strogatz, Phys. Rev. E **67**, 036204 (2003).

Figure captions

Fig. 1: Variance σ^2 as a function of k for several parameters of γ as computed from Eq. (21). For $\gamma \to \gamma_c$ the variance of the critical mode with $k_c = 0$ tends to infinity, whereas the variances of all other modes remain finite. Control parameters (from bottom-up): $\gamma = 1.00$, $\gamma = 1.02$, $\gamma = 1.04$. Other parameters: $\tau = 1.0$, $t_0 = 1.0$, $g_e = 0.2$, $g_i = 2.0$, $Q = 1.0$, $R = 10$, $D = 4giR^2/[g_e\pi^2]$ and $\gamma_c = 1.05$.

Fig. 2: Evolution of the first moment $M_1(t)$ of the critical mode $k_c = 0$ computed from Eq. (19) for two cases: $\gamma = 0.9 < \gamma_c$ (dashed line) and $\gamma = 1.1 > \gamma_c$ (solid line). Other parameters as in Fig. 1.

Fig. 3: Real part of the Lyapunov spectrum $\lambda(k)$ at the bifurcation point $\gamma = \gamma_c$ as obtained from Eq. (24) for a particular set of parameters. Critical modes with $\lambda(k) = 0$ occur at $k = \pm k_c$ and $k_c > 0$. Parameters: $\tau = 1.0$, $g_e = 1.0$, $g_i = 0.2$, $r_e = 0.2$, $r_i = 1.0$, $v = 1.0$, and $\gamma_c = 1.158$.

Fig. 4: Upper band of Fig. 3. The critical modes are at $k = \pm k_c$ and $k_c \approx 1.2$. The homogeneous Fourier mode is stable at the critical point (i.e. $\lambda(0) < 0$).

Fig. 5: Variance $\sigma^2(k)$ as obtained by solving Eq. (23) numerically for $\gamma = 1.0$ and $\gamma = 1.1$ (from bottom-up) using an Euler forward scheme [49]. The variance has a maximum at the critical mode $k_c = 1.2$. Other parameters as in Fig. 3.

Fig. 6: Evolution of the first moment $M_1(k_c, t)$ of the critical mode with $k_c = 1.2$ computed from Eq. (25) for $\gamma = 1.0 < \gamma_c$ (dashed line) and $\gamma = 1.17 > \gamma_c$ (solid line). For $\gamma = 1.17 > \gamma_c$ the first moment $M_1(0, t)$ of the homogeneous Fourier mode is shown as well (diamonds). The homogeneous Fourier mode is stable, whereas the critical mode is unstable. Other parameters as in Fig. 3.

Fig. 7: The log-log-plot of the power spectrum from Eq. (26) for two parameter sets. Further parameters are $k_0/\sqrt{D} = 200.0$, $Q/2\pi\sqrt{2\pi D} = 1.0$.

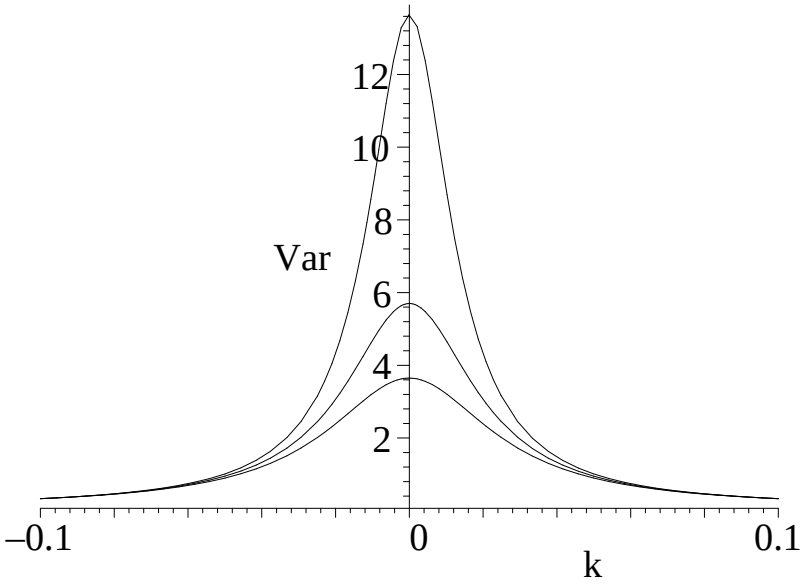

FIG. 1:

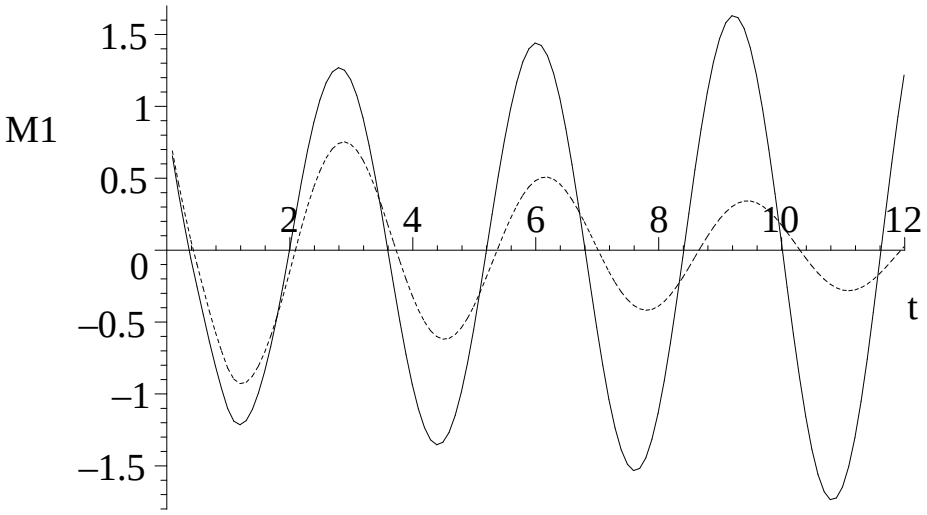

FIG. 2:

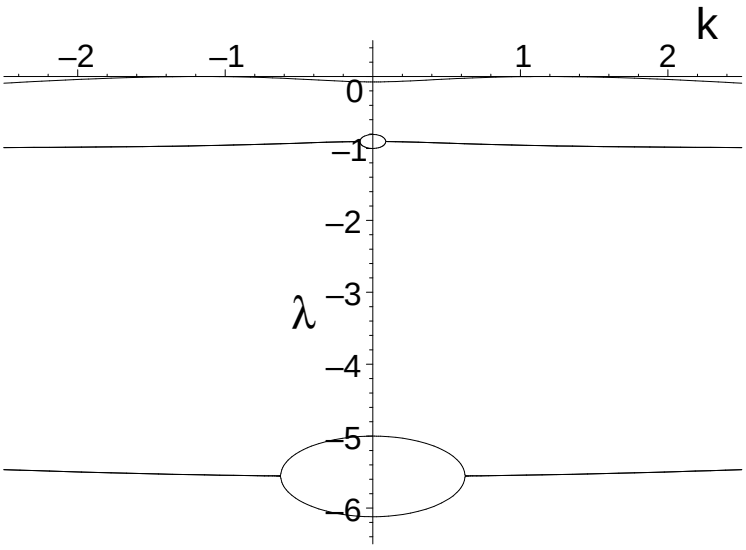

FIG. 3:

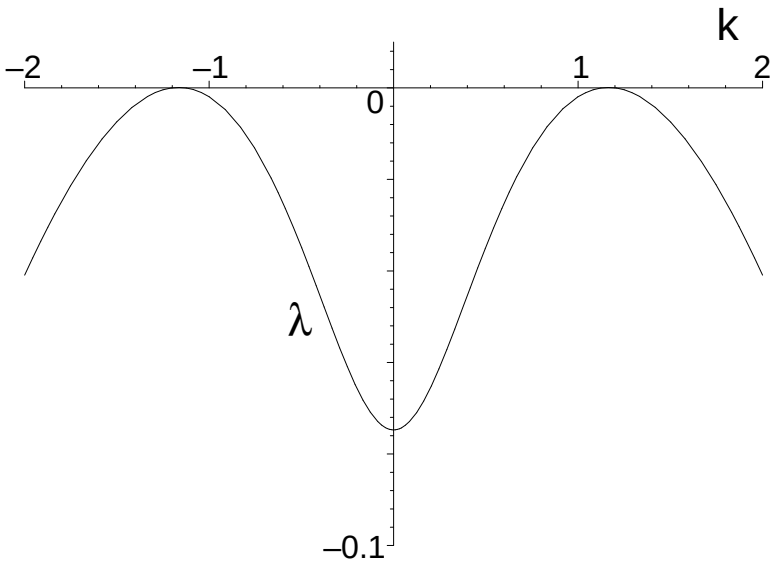

FIG. 4:

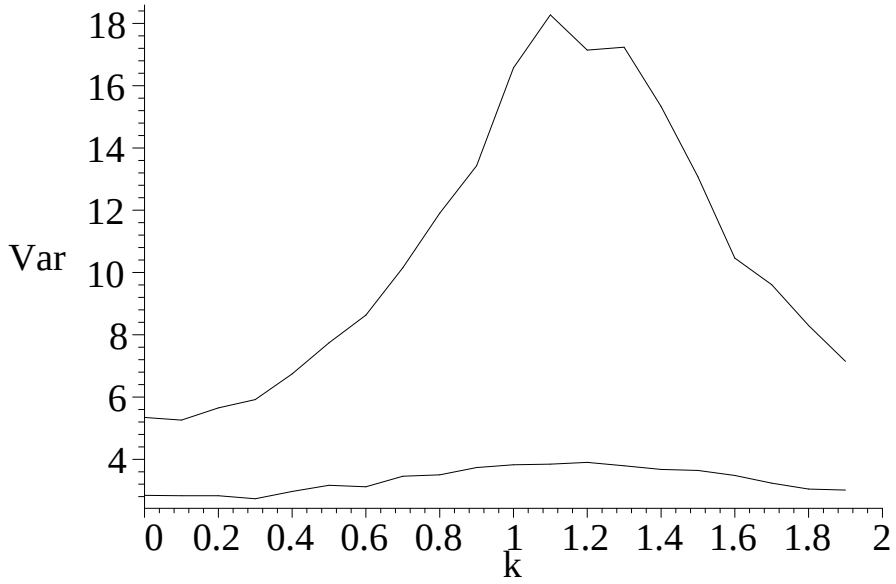

FIG. 5:

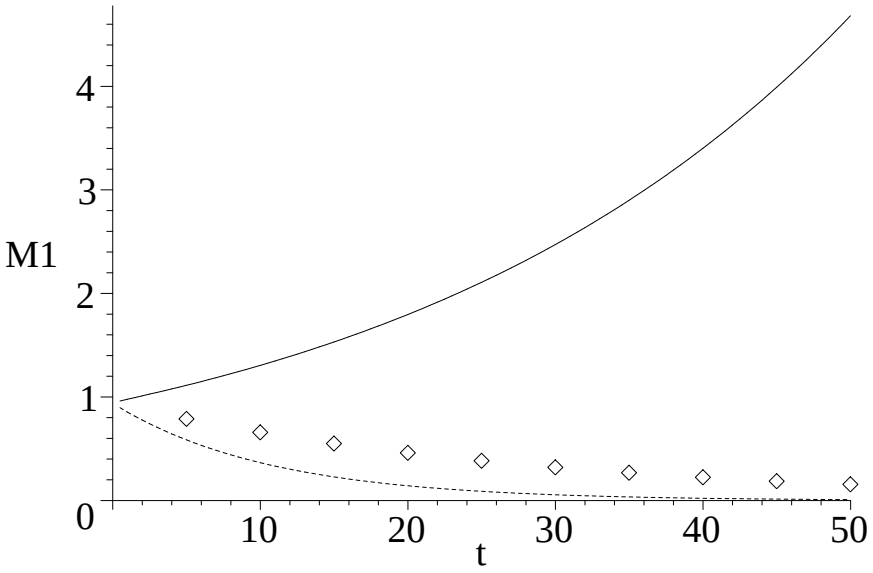

FIG. 6:

FIG. 7: